

Retraction

Retracted: Digital Technology Empowers Grain Supply Chain Optimization Simulation

Complexity

Received 23 January 2024; Accepted 23 January 2024; Published 24 January 2024

Copyright © 2024 Complexity. This is an open access article distributed under the Creative Commons Attribution License, which permits unrestricted use, distribution, and reproduction in any medium, provided the original work is properly cited.

This article has been retracted by Hindawi following an investigation undertaken by the publisher [1]. This investigation has uncovered evidence of one or more of the following indicators of systematic manipulation of the publication process:

- (1) Discrepancies in scope
- (2) Discrepancies in the description of the research reported
- (3) Discrepancies between the availability of data and the research described
- (4) Inappropriate citations
- (5) Incoherent, meaningless and/or irrelevant content included in the article
- (6) Manipulated or compromised peer review

The presence of these indicators undermines our confidence in the integrity of the article's content and we cannot, therefore, vouch for its reliability. Please note that this notice is intended solely to alert readers that the content of this article is unreliable. We have not investigated whether authors were aware of or involved in the systematic manipulation of the publication process.

Wiley and Hindawi regrets that the usual quality checks did not identify these issues before publication and have since put additional measures in place to safeguard research integrity.

We wish to credit our own Research Integrity and Research Publishing teams and anonymous and named external researchers and research integrity experts for contributing to this investigation.

The corresponding author, as the representative of all authors, has been given the opportunity to register their agreement or disagreement to this retraction. We have kept a record of any response received.

References

- [1] X. Xu and Z. Sun, "Digital Technology Empowers Grain Supply Chain Optimization Simulation," *Complexity*, vol. 2021, Article ID 6496713, 12 pages, 2021.

Research Article

Digital Technology Empowers Grain Supply Chain Optimization Simulation

Xiaoyan Xu ^{1,2} and Zhongye Sun ¹

¹Food Science and Engineering, Department of Economic and Trade, Henan University of Technology, ZhengZhou 450001, China

²Zheng Zhou Institute of Science and Technology, ZhengZhou 450064, China

Correspondence should be addressed to Xiaoyan Xu; 201791013@stu.haut.edu.cn

Received 9 April 2021; Revised 21 May 2021; Accepted 15 June 2021; Published 23 June 2021

Academic Editor: Zhihan Lv

Copyright © 2021 Xiaoyan Xu and Zhongye Sun. This is an open access article distributed under the Creative Commons Attribution License, which permits unrestricted use, distribution, and reproduction in any medium, provided the original work is properly cited.

The issue of the balance of food supply and demand has always been the main issue of national and even world food security. There are many factors that affect food supply and demand, and the factors are interrelated. Therefore, it is necessary to study this complex issue in a systematic way in order to provide a reliable theoretical basis for the country to formulate effective policy measures. Based on the analysis of the current situation of grain supply and demand, this paper uses system dynamics (SD) to carry out digital elevation model (DEM) and latitude correction for land surface temperature (LST). The LST, combined with the normalized difference vegetation index (NDVI), has initially constructed a temperature vegetation dryness index (TVDI) model; it has constructed five subsystems including arable land, production capacity, import, population, and consumption. This paper proposes a food supply chain network construction model from the dimensions of the food supply chain network's information flow, logistics, and business flow. Through detailed empirical analysis of each subsystem, we judge the development trend of the total grain system, perform operational tests and historical tests on the simulation results of the model to judge the rationality of the model system structure and simulation prediction, and give the simulation results. Finally, based on the forecast results, targeted countermeasures and suggestions are proposed.

1. Introduction

As of 2018, the national food production has shown a continuous growth trend for 11 years. Although the national food production declined slightly in 2019, it was still at the second level in the past years [1]. The adjustment of the planting industry structure has achieved initial results, but due to the rapid development of urbanization, the country's agricultural arable land area is also declining [2]. The development of information technology and its practical application in the agricultural field is the fundamental way to ensure the sustainable and stable development of agriculture and ensure the long-term high-quality supply of agricultural products [3]. Therefore, studying the possible damage to the food supply network and analyzing the impact of the network damage on the food supply are of great significance for the preparation of emergency plans for food supply in

emergencies and the development of effective food supply network security strategies. An information agriculture technology system suitable for national conditions is researched and created, farmland sensor technology and agricultural Internet of Things technology are vigorously developed, and real-time monitoring and control of crops are realized [4]. At the same time, the population base is too large, and people's dietary structure has undergone tremendous changes [5]. Nowadays, the supply of rations can be absolutely sufficient, but the amount of feed and industrial use has increased significantly, and the country's domestic food supply gap has been expanding [6].

There are many studies on food security, and scholars have their own research focuses. The research results also provide a certain theoretical support for national food security [7]. Traditional farmland information acquisition is mainly through manual sampling and indoor chemical

analysis, which is not only time-consuming and labor-intensive but also low in efficiency [8]. With the development of sensor technology, it is possible to detect farmland information through farmland sensors. Experts and scholars at home and abroad have also done a lot of experimental research in the field of farmland information acquisition [9]. In terms of obtaining crop growth information, the SPAD-502 chlorophyll sensor produced by Japan's MINOLTA company uses light-emitting diodes to emit red light and near-infrared light. The obtained electrical signal is derived from the measurement result [10]. Balderas [11] found that there is a significant linear correlation between the measured value of the chlorophyll meter and the total nitrogen content of winter wheat plants and proposed a crop nitrogen nutrition evaluation based on the measured value of the chlorophyll meter. For the study of chlorophyll, Zhu et al. [12] showed that the chlorophyll density information of the colony vegetation can be obtained through the position information of the "red edge" of the spectrum. Scholz et al. [13] showed that the chlorophyll content of corn in the V6 growth stage can be predicted by the spectral reflectance model. Zhong et al. [14] established a linear detection model for chlorophyll content at the jointing and booting stages according to the coordinates of the red edge inflection point of the canopy reflectance spectrum. Using machine vision technology, Tordecilla et al. [15] studied the color changes caused by lack of water and nitrogen in plants, indicating that color is an effective classification feature that can be used to identify plants and leaves. Lohmer et al. [16] established a rice mid-term nitrogen fertilizer management and yield prediction system based on machine vision. Researchers studied computer vision technology and used it to diagnose the nutritional status of cucumber growth, collected greenhouse cucumber leaf images, detected the nutritional information of the leaves, and found that the leaf green component G and chromaticity H component are linear with the nitrogen content; it can be used as a machine vision to quickly diagnose cucumber growth indicators [17]. In the field of spectral analysis applications, many experts have systematically analyzed the relationship between spectral characteristics and plant nitrogen nutrient content. Studies have shown that the spectral emissivity analysis of corn canopy in different growth periods has been carried out using spectral analysis techniques, and the trend of reflectivity changes in the visible and near-infrared regions at different growth periods of maize is pointed out [18]. It gradually increases in the visible light range and gradually decreases in the near-infrared region [19].

Some scholars are doing nitrogen difference gradient experiments for different wheat varieties, showing that the differential spectrum of the canopy changes regularly with the increase in nitrogen level in the red border area. The sum of the first-order differential in the red frame and the measured value of nitrogen accumulation in wheat is calculated, and the coefficient R^2 reaches 0. At the same time, the red edge feature parameters were used to detect the nitrogen content of rice leaves [20]. Studies have shown that the use of multispectral and hyperspectral imaging technologies can achieve rapid nondestructive detection of crop

nitrogen content [21]. Some researchers have proposed an accurate variable management system for corn nitrogen content based on ground-based multispectral image technology, with a correlation coefficient (R^2) of 0.89. Some experiments used CCD cameras and filters to obtain multispectral images to detect the nitrogen content of cucumber leaves. The results showed that there is an obvious linear correlation between NDVI and leaf area and leaf nitrogen content [22]. Phosphorus and potassium are also very important for crop growth. Studies have shown that the use of machine vision technology to extract the leaf characteristics of the color image of the leaves of the tomato grown under soilless cultivation under nitrogen and potassium deficiency can ideally identify the nutrient-deficient tomato leaves [23]. By extracting the color and texture information of the nutrient-deficient tomato leaves, the recognition rate reaches 92.5%–95%, and it can be recognized 6–10 days earlier than the naked eye [24]. Using spectral analysis technology, by observing the canopy spectral reflectance of hydroponic potted rice with different potassium nutrient levels, scholars found that the effect of potassium on the spectral characteristics of the canopy is similar to the effect of nitrogen. The spectral reflectance is reduced, and the spectral reflectance of the near-infrared band is significantly increased [25]. Some researchers believe that Monte Carlo simulation and diffuse reflectance spectroscopy can be used to establish a tomato nutrient supply model and analyze the intrinsic relationship between nutrient elements and near-infrared spectroscopy [26].

In the context of the current situation of supply and demand, this article subdivides national food security issues into five major sectors: arable land, production capacity, imports, population, and consumption. Wireless sensor network is the most important implementation method of the underlying network in the Internet of Things architecture. It consists of various wireless sensor nodes installed in the farmland area. These sensor nodes are connected to each other in the field to form a multihop self-organizing network for real-time collection and transmission. Therefore, for farmland wireless sensor networks, research on sensor calibration methods and data processing is a prerequisite for improving the accuracy of farmland perception data and ensuring the reliable implementation of agricultural production management decisions. This paper takes farmland soil moisture sensors, farmland CO₂ sensors, and crop growth sensors as the research objects and aims to improve the accuracy of farmland perception data. The methods of farmland sensor correction and perception data cleaning are studied, and the factors that affect the measurement accuracy of farmland sensors are analyzed. The main factors clarified the necessity of farmland sensor calibration. Taking farmland soil moisture sensors, farmland CO₂ sensors, and crop growth sensors as the research objects, the above three farmland sensors were calibrated using the least square algorithm and BP artificial neural network algorithm, and the calibration results were compared and analyzed. According to the characteristics of the food supply chain network, two indicators of invulnerability are proposed, namely, network security and network average efficiency

indicators. The results showed that both the least square algorithm fitting and the BP artificial neural network algorithm fitting can correct the calibration data of farmland sensors, but the linearity of the BP artificial neural network fitting is compared with the linearity fitted by the least square algorithm. If it is smaller, the nonlinear J-wa calibration effect is more significant. In terms of accuracy, the BP artificial neural network algorithm is better than the least square algorithm.

2. Digital Technology Empowers Food Supply Chain Model Construction

2.1. Fundamentals of Digital System Agricultural Biology. When crops grow normally, based on the data obtained by satellite remote sensing, vegetation index, vegetation canopy temperature, and other values are kept within a certain normal range; when crop water supply is insufficient or uneven, its growth is affected and the vegetation index decreases. When some nodes or edges of the grain supply chain network suffer random or deliberate attacks and fail, it will indirectly affect the function of the grain supply chain network. The water supply for the transpiration of vegetation leaves is insufficient, the stomata of crop leaves are closed, the transpiration is reduced, and the crop canopy temperature rises [27–33]. By comprehensively considering the two indicators of vegetation index and vegetation canopy temperature, the vegetation water supply index (VWSI) is the simple ratio of the vegetation index (NDVI) to the crop canopy temperature (T_0) and then multiplied by an image enhancement coefficient (B). The specific formula is as follows:

$$VWSI = \frac{B * (NDVI)}{T_0}. \quad (1)$$

Among them, the vegetation index is directly proportional to the leaf area index. The better the crop is, the larger the vegetation index is; the vegetation canopy temperature is directly proportional to the water supply [34, 35]. When the crop is under water stress, the canopy temperature increases and the VWSI value decreases. The smaller the VWSI value, the less the soil moisture of the crops and the more serious the agricultural drought. Temperature vegetation drought index (TVDI) comprehensively considers the vegetation index and the surface temperature and studies the relative drought degree and change characteristics of the region in a specific time period:

$$TVDI = \frac{(LST(NVDI) - LST(\min))}{(LST(\max) - LST(NVDI))}, \quad (2)$$

$$LST(NVDI) = A + B * NVDI.$$

Conditional temperature vegetation index is similar to TVDI; it studies the relative drought in a certain time period:

$$\begin{aligned} LST(\min) &= a1 + b1 * NVDI, \\ LST(\max) &= a2 + b2 * NVDI. \end{aligned} \quad (3)$$

A , b , $a1$, and $b1$ are the coefficients of the fitted dry and wet edges; LST -max and LST -min are the fitted dry and wet edge equations, respectively, representing the maximum and minimum values of LST corresponding to the $NDVI$ value of a certain pixel. In formula (3), $a2$ indicates that the supply chain network has m nodes and $b2$ is the set of edges of each node in the network. The larger the $TVDI$ value, the more severe the relative drought in the region.

As far as the vegetation coverage of the entire study area is concerned, the characteristic space formed by the surface temperature and vegetation index from bare land to high vegetation coverage area is in a triangular or trapezoidal relationship. It was originally used to study vegetation transpiration. In the research of slow infiltration of soil water content, current scholars use this model to monitor agricultural drought. The two index data of vegetation index and surface temperature are selected to construct the T_s -VI feature space, which is composed of the temperature value corresponding to the $NDVI$ value in a certain period of time in the study area. In addition, it can be seen that when the $NDVI$ value is the smallest, the corresponding maximum LST value is the largest, and the vegetation transpiration is 0. At this time, as the maximum LST value decreases (from point A to point B), it evaporates.

$$\log(LST(k)) = \log(LST(k-h)) + f(k). \quad (4)$$

According to the constructed feature space, it can be seen that the larger the value of $b1$, the larger the $TVDI$ value and the larger the corresponding T_s value at this time. Because the high surface temperature is a manifestation of the low soil moisture content, it indicates that the drought is more serious at this time; when the value of $b1$ is smaller, the $TVDI$ value is smaller, and the corresponding T_s value is smaller, and the low surface temperature indicates that the soil is moist at this time; and when $b1 = b2$, the $TVDI$ value is the largest, indicating that the drought is the most serious; and when the value of $b1$ - $b2$ is larger, the area of the characteristic triangle area is larger, and the drought grade is clearer. Therefore, the larger the $TVDI$ value, the more severe the drought; the smaller the value, the slower the drought. Since $T_s \leq T$ -max, the value range of $TVDI$ is $[0, 1]$.

2.2. Correction Algorithm Based on Digital Least Squares Fitting. BP (back-propagation) neural network is a feed-forward artificial neural network. It was proposed in 1986 by a team of scientists led by Rumelhart and McClland. It is currently one of the most widely used neural network models. The BP network learns and stores a large number of input-output mapping relationships without knowing the internal mechanism or function equation. The topological structure of the BP artificial neural network model consists of an input layer (input), a hidden layer (hidden layer), and an output layer (output layer). The learning process of BP artificial neural network is divided into forward propagation process and error back-propagation process. Information is transferred from the input layer to the output layer through the hidden layer. This shows the management characteristics

of the food supply chain network. Therefore, the food supply chain network is a typical super network. If the desired output value is not obtained in the output layer, it will follow the original path. The error returns and modifies the weights of the neurons in each layer so as to minimize the error and finally achieve the desired effect.

The output of each neuron in this layer is equal to the hidden layer. The input value of each neuron in the hidden layer is the weighted sum of the output value of the previous layer.

$$f(k) = \frac{a0}{(1 + \exp(k))}, \quad (5)$$

where $f(j)$ is the threshold; it is the connection weight from the input layer to the hidden layer. It is the output layer of the hidden layer; the output layer uses a linear function, and the output value is the weighted sum of the input values.

$$u = (\text{LST}, \text{NVDI}, k, h)^T. \quad (6)$$

Among them, V is the connection weight from the hidden layer to the output layer. $u(k)$ is the threshold of the output layer. Back-propagation process error function definition is as follows:

$$\begin{bmatrix} u(k) \\ u(h) \end{bmatrix} = \begin{bmatrix} f(k, h) + w(k) \\ \text{LST}(k) \end{bmatrix}. \quad (7)$$

In the formula, k and h , respectively, represent the adjacency matrix of the supply chain network node and $f(k)$ and $w(k)$ are the flow set of each edge in the network of each node edge in the network. The gradient descent method is used to sequentially adjust the correction amount of the output layer weight, the correction amount of the output layer threshold, the correction amount of the hidden layer weight, and the correction amount of the hidden layer threshold.

According to the test standard data x and the measurement data Y , a set of nonlinear curves $Y=f(x)$ is obtained, and the inverse nonlinear curve $x=f$ is approximated by a polynomial of degree n , and then the coefficients of the polynomial are obtained by the principle of the least square algorithm. List the n - t - h degree polynomials, and set the 11th degree polynomial equations. Since it is data calibration for farmland sensors, the actual situation of the accuracy requirements of farmer's emotional knowledge data can be considered. Since the value of the parameter is unknown, we regard it as a random variable; then, before observing the specific training sample, it can be represented by a prior probability density function p . According to the related discussion of posterior probability density, we know that p has a very significant peak near the true value. According to the principle of least squares, the coefficient a can be obtained when the mean square error between each y - f and the corresponding standard value X - f is the smallest. Solving the fitting function using Cramer's rule to solve Formula (7), the coefficient a can be solved, and then the fitting parameters can be solved. The specific algorithm is shown in Figure 1.

The segmentation clustering method starts by randomly extracting a certain number of data instances from the object data set as the prototype of the clustering. The security of food supply is the primary factor that should be considered in the design and operation of the food supply chain network. After the first step is completed, the remaining data instances are allocated to the subset represented by the prototype. The segmentation cluster uses repeated iterations to adjust the original data. TensorFlow uses Tensor to represent data, and TensorFlow internally represents tensors as n -dimensional arrays of basic data types. This process is repeated until the analysis effect reaches the best. The most representative example is to make the average distance between each data instance and its original data reach the lowest value.

The solution is proposed to solve this problem; the algorithm steps are as follows. (1) Arrange the first data instance into the first group. (2) Assign the next data instance, and arrange it into an existing group or a new group according to specific rules. Usually at this time, every time you add a new data instance to the group, you need to recalculate the criterion function on which the allocation is based to ensure that it always meets the requirements. (3) Loop the first two steps until all the data are analyzed. The incremental algorithm does not require much memory and only requires the provision of necessary allocation rule functions to complete the allocation of data instances. The difference is that the incremental algorithm does not need to be iterative, so it has the advantage of faster speed compared with other algorithms. However, a major disadvantage of the incremental algorithm is that the algorithm is greatly affected by the order of the data instances. If the order of the data instances changes, the results of the incremental algorithm are also very different. The reason why the density-based clustering method is different from the previous clustering algorithms is its characteristic of judging based on local data characteristics. Complex network theory usually uses the average shortest path index of the network to represent the fragility characteristics of the network, and the average value of the shortest path between any two nodes in the network is called the average minimum risk path. Consider a data subset or grouping as a data range, and divide the data instances within the range according to their density. Most density-based clustering algorithms do not have a specific scope for the shapes formed by their clusters. Figure 2 shows the framework of the digital technology empowered food supply chain model.

2.3. Model Parameter Optimization. According to research, in addition to the two main factors required to establish the model, the factors that affect the accuracy of the TVDI model, the surface temperature and vegetation coverage, the uncertainty of solar radiation, and atmospheric conditions have a certain degree of influence. In order to facilitate the description of the complete destruction of the network, the average value of the sum of the reciprocal of the average shortest path value between nodes is called the network

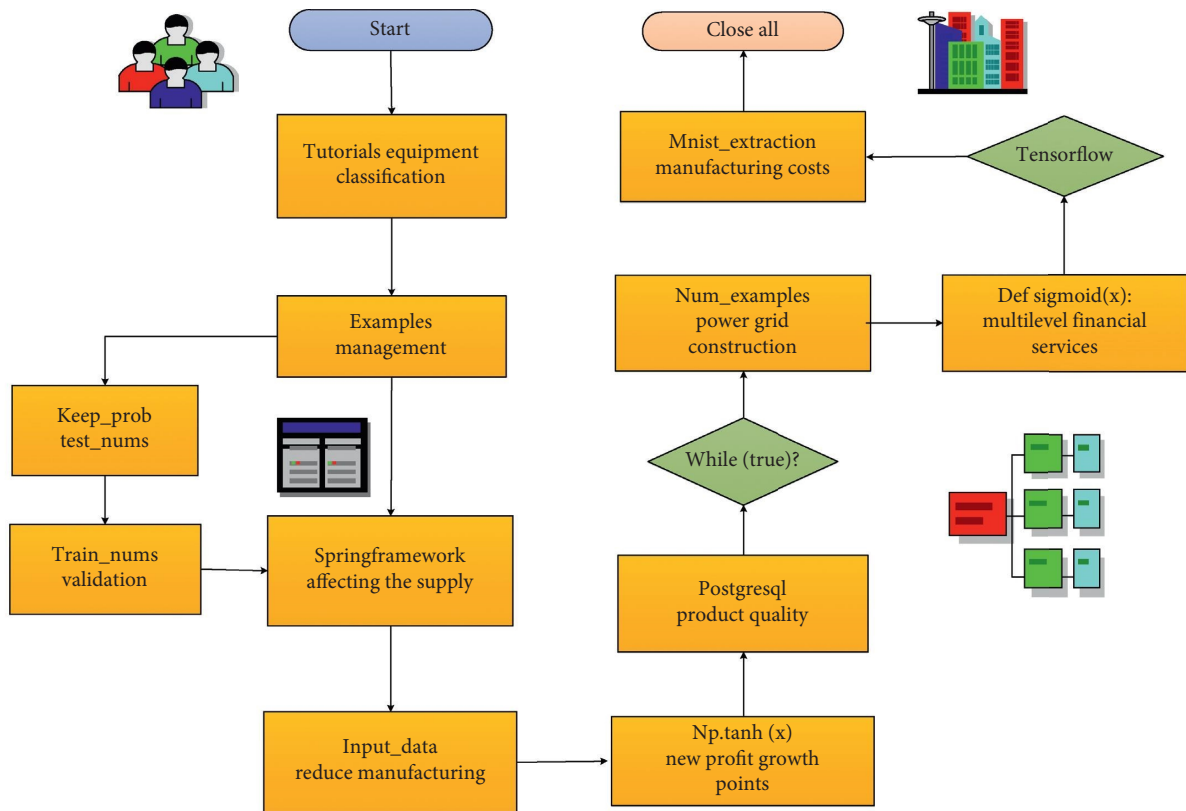


FIGURE 1: The flow chart of the correction algorithm based on digital technology least squares fitting.

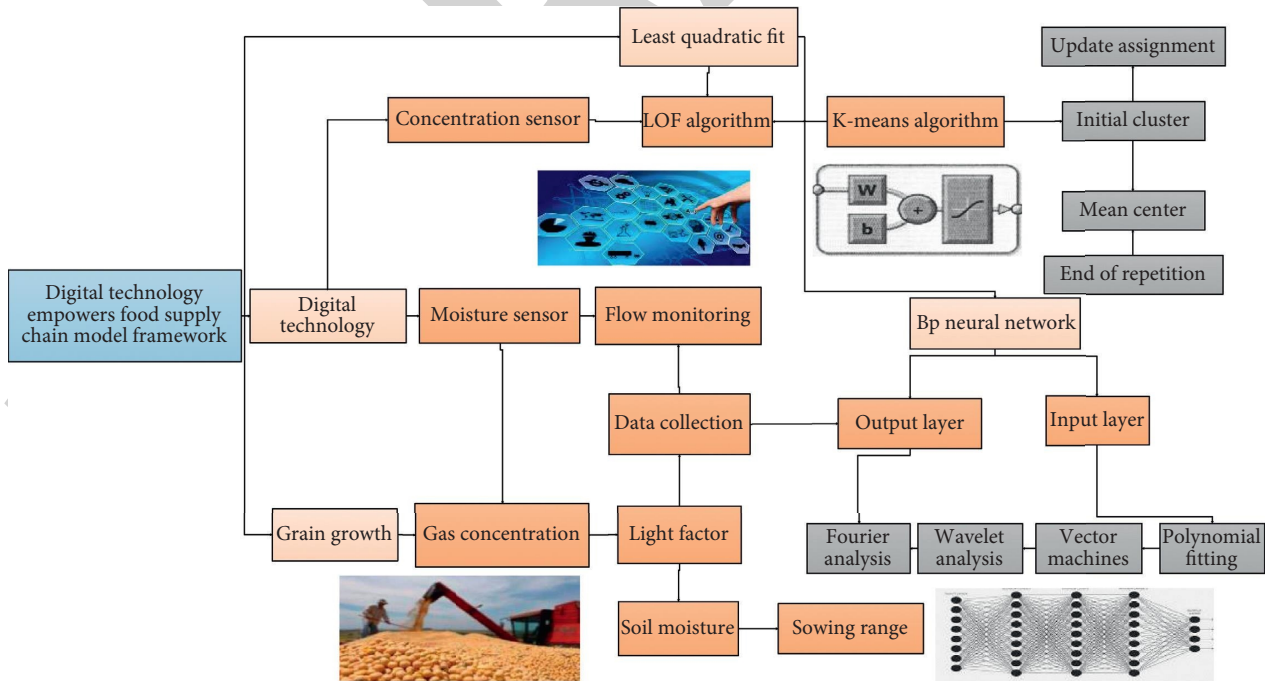


FIGURE 2: Digital technology empowered food supply chain model framework.

security efficiency index. The northern and central parts are dominated by mountainous areas. The basins are concentrated in the south. The hills are low in temperature and the basin is high in temperature, which can easily lead to the

wrong analysis of “low drought and high humidity.” Therefore, the DEM and latitude must be corrected to obtain accurate surface temperature. For areas with higher altitudes, the temperature decreases as the elevation increases,

and the LST will also decrease under the influence of temperature, resulting in higher estimates of soil water content and drought prediction.

The experiment uses random node deletion, edge deletion method, and deletion method based on the order of the magnitude of the median value to simulate random destruction and deliberate attack. In order to avoid or reduce the influence of altitude, DEM correction is made to LST; the specific formula is $T2 = T1 + m1 \times H$ where $T1$ and $T2$ are the surface temperature before and after DEM correction; $m1$ is the surface temperature coefficient of temperature affected by DEM and is taken as an empirical constant $0.6/100$ °C/m; and H is the elevation of the pixel point/m, and the specific digital temperature data distribution of different grain sample groups is shown in Figure 3. We carry out latitude correction of the surface temperature in the middle and high latitudes; due to the increase in latitude, the temperature decreases and the surface temperature decreases, leading to higher estimates of soil water content and lower drought predictions than the real situation. In order to avoid or weaken the influence of latitude, add latitude correction to LST, and the specific formula is $T3 = T2 + m2 \times a - b$ where $T3$ is the surface temperature after elevation or elevation and latitude correction; $m2$ is the correction coefficient of the surface temperature that varies with latitude; a is the latitude of the pixel; b is the minimum latitude in the study area; and $m2$ is taken as the empirical constant 0.9413 °C. It is considered that for every 1° increase in latitude, the temperature will decrease by 0.9413 °C; the value of a is taken as the minimum latitude of a province of $34^\circ 36'$. The realization of latitude correction requires the help of IDL tools to calculate the image pixel by pixel; that is, it is considered that for each pixel increase with latitude, the temperature decreases by t . The experiment uses the survivability model indicators of the food supply chain network to perform simulation calculations under different network attack strategies to measure the network survivability, and then we take 7 samples separately. Among them, l-max and min are the maximum or minimum latitude in the study area and n is the number of pixel rows. Figure 4 shows the statistical fitting error of the vegetation index numbers.

When constructing the Ts-VI feature space, the fitted dry edge and the real dry edge are greatly affected by vegetation. Because the soil in the bare soil area will be extremely dry, the pixel points on the dry edge of the bare soil may have soil moisture content. However, in areas with high vegetation coverage, the soil moisture content will not be zero due to vegetation coverage, so the soil moisture of the pixels located on the dry side must not be zero. The surface temperature of the pixel points on the dry edge fitted by remote sensing data is lower than that of the real dry edge, and the higher the vegetation index, the greater the error of the dry edge fitting. In the simulation experiment of this paper about l-min, corresponding to the data points on the blue and red lines, respectively, the random attack strategy adopts deleting one node at a time and taking the average value continuously for 5 times. The lower the vegetation index, the smaller the fitting error. The change in the mean value of supply variables is shown in Figure 5. Therefore, it is necessary to

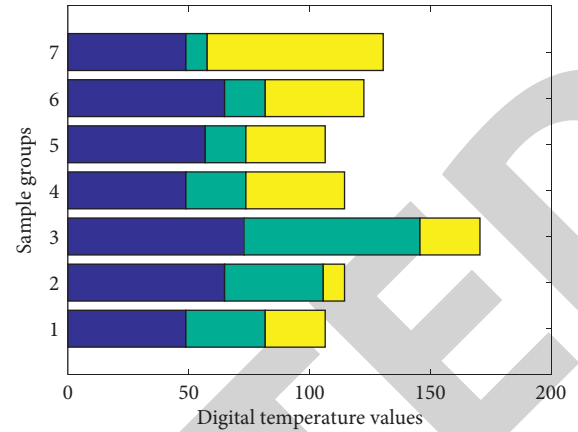


FIGURE 3: Distribution of digital temperature data for different grain sample groups.

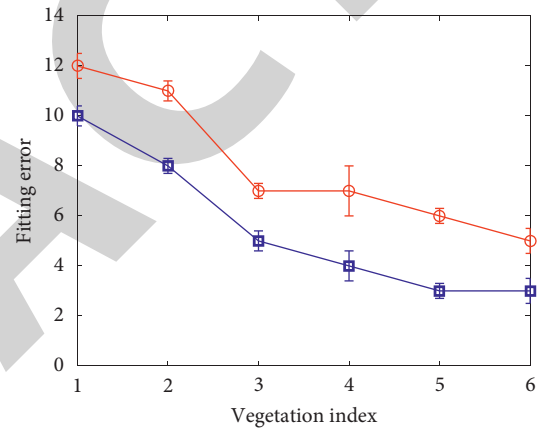


FIGURE 4: Statistical fitting error of vegetation index numbers.

correct the dry edges of the feature space. The density-based outlier detection algorithm judges the similar data instances with low density as outliers. There are two main types of density-based outlier detection algorithms. For example, the LOF out-layer detection algorithm uses the distance information of the k nearest neighbors of the data object to calculate the local data density because it is necessary to find the k nearest neighbors of each data point in the data set.

3. Application and Analysis of Digital Technology Empowered Grain Supply Chain Model

3.1. Digital Simulation of Food Supply Chain. TZS-W type portable soil moisture meter is a high-precision soil moisture meter produced by Top Instrument Co., Ltd. It can directly measure the soil moisture value and can also record the time and moisture content of each sample during the measurement in real time. The data can be exported by connecting with the computer, and the moisture distribution can be analyzed in the computer. The HL is used by the farmland information wireless sensor node. The deliberate attack strategy is to delete nodes and edges in the order of the betweenness numbers. When encountering multiple identical nodes and edges, one

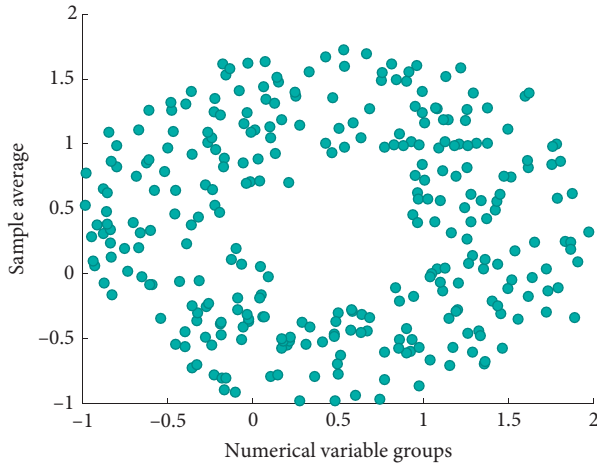


FIGURE 5: Scattered distribution of the mean value of food supply variables.

of them is randomly selected. The proportion of each factor is shown in Figure 6. It is a high-precision, high-sensitivity sensor for measuring soil moisture based on the principle of frequency domain reflection and using high-frequency electronic technology. By measuring the dielectric constant of the soil, it can directly and stably reflect the volume percentage of the real soil moisture in various soils. It is currently the most popular soil moisture measurement method.

Let us calculate the distance from each sample to the mean center, arrange the distance in descending order, and list the 10 abnormal points with the largest distance in the results of the detection algorithm. The sample numbers corresponding to the abnormal points are 3166, 3326, 2716, 3457, 2896, 2707, 3237, 2661, 3323, and 3239; the data fitting of the grain supply sample is shown in Figure 7. It can be found that the CO₂ concentration value is much lower than other monitoring values nearby. Under the deliberate destruction based on the intermediate value marked as each sample, the security performance of the network declines more rapidly than the random destruction. Combined with the actual situation, we can judge that this is an outlier removed.

Because it is a calibration test, the soil moisture value measured by the W-type portable soil moisture meter is the standard value and set as x ($x = 1, 2, 3, \dots, n$), using the HL used by the farmland information wireless sensor node. The soil moisture content measured by the TR01 soil moisture sensor is the measured value, which is set to t ($t = 1, 2, 3, \dots, n$). The connection weights from the input layer to the hidden layer are $w = [-14.0693, 12.4547, 7.1395, 11.0440, 14.8659, 13.9138, 13.6723, 13.5017, 14.0008]$; the threshold from the input layer to the hidden layer is $\text{net-b} = [13.8078, 9.7433, -5.9292, 4.4684, 1.9577, 2.2440, -5.3568, 7.6694, -10.9388, 14.3411, 13, 0.6583]$; the connection weights from the hidden layer to the output layer are $w = [0.5571, 0.653, 0.5301, 0.1270, 0.2550, 0.1574, 0.0889, 0.0137, 0.1429, 0.3982]$. Under the action of deliberate destruction, when the node deletion ratio is 0.682, the security value on three curves of the network drops to 0, indicating that the network

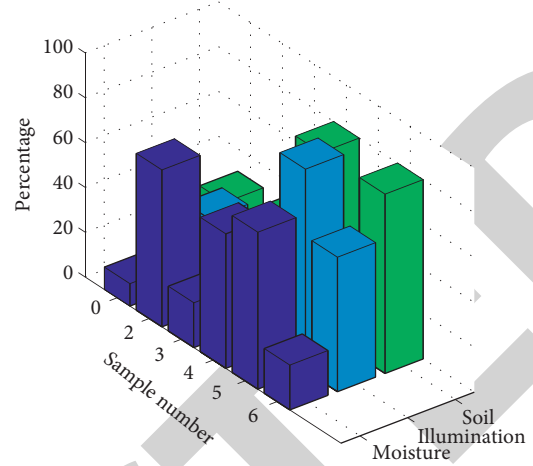


FIGURE 6: Proportion of factors affecting food supply.

is completely destroyed. The detection values of the digital sensors of different food samples are as shown in Figure 8; the BP artificial neural network model is obtained through these 20 sets of data training.

Use 10 sets of data as test data, and use these 10 sets of data to test the performance of the model. The remaining 10 sets of data are used as test data, and the stability of the BP artificial neural network model is tested by testing these 10 sets of data. Through training, the final number of iterations of the BP artificial neural network epoch is 90, the correlation coefficient between the training data sets is 0.9978, the correlation coefficient between the verification data sets is 0.99386, the correlation coefficient between the test data sets is 0.999142, and the overall correlation coefficient is 0.9493, as shown in Figure 9, and the fitting correlation $R^2 = 0.99$, and the fitting curve corrected by the BP artificial neural network is obtained.

3.2. Experimental Results and Analysis. According to the research content and purpose, two kinds of remote sensing data of vegetation index and land surface temperature are used. MODIS data products have the characteristics of high time and medium and high spatial resolution. Since their launch in 2000, they have become the main data used in large-scale remote sensing research. Therefore, the data source for the study from 2001 to 2016 uses the MODIS 13Q1 vegetation index product. In 2020, NOAA/AVHRR Pathfinder data will be adopted. The time period is from 1984 to 2000, and the long-term national vegetation index data set (AVHRR_Path-Finder) of the Science Data Center for Cold and Arid Regions is used. The vegetation index data are NDVI data with a spatial resolution of 8 km and a temporal resolution of ten days. MODIS product data are divided into 44 types. System dynamics can be combined with other software for simulation and simulation. This article uses Vensim software. Vensim simulation software is a multi-functional software developed by Ventana Systems in the United States. The download address of this type of standard data is a website, and the downloaded data format is HDF. Figure 10 shows the polar coordinate display of grain sample

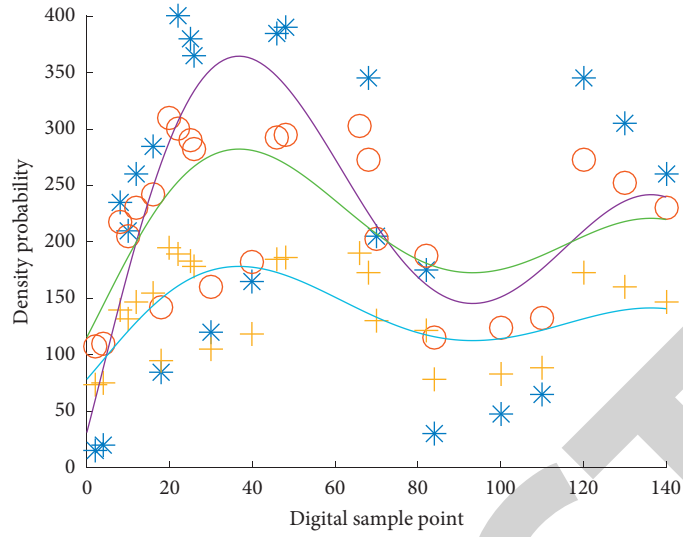


FIGURE 7: Data fitting curve of food supply sample.

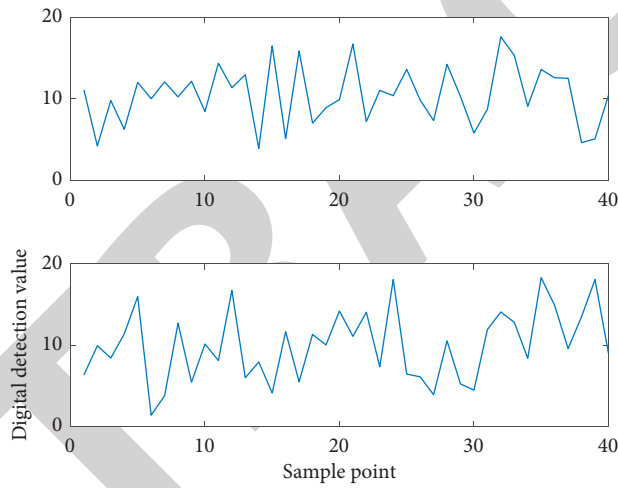


FIGURE 8: Digital sensor detection values of different grain samples.

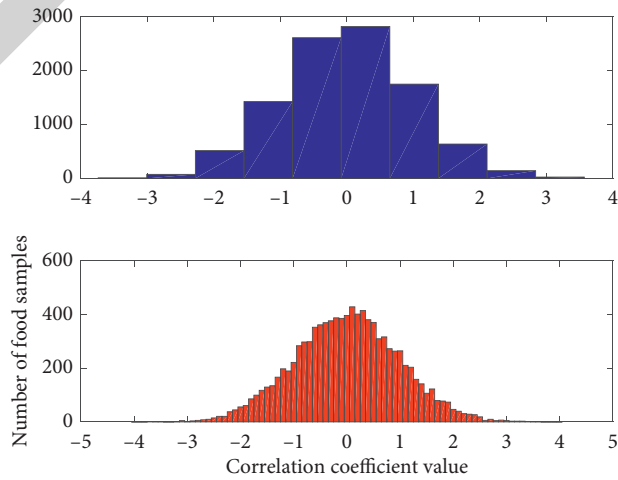


FIGURE 9: Statistical distribution of correlation coefficients of grain supply after model correction.

collection data. The vegetation index data used in this article are MOD13A2, a terrestrial tertiary product, with a spatial resolution of 1 km and a temporal resolution of 16d.

Corresponding to vegetation index data, land surface temperature (LST) data are also divided into two types according to time periods. (1) NOAA/AVHRR Pathfinder data: The period is from 2014 to 2000; using the Path-Finder data set of the Cold and Arid Regions Science Data Center, based on the CH4 and CH5 channel, calculate brightness temperature data included in the data set in Figure 10. The spatial resolution is 8 km, and the temporal resolution is ten days. (2) MODIS data: The time period is 2001–2016. The surface temperature data product (MOD13A2) of the MODIS data products provided by NASA's official website is a terrestrial tertiary product, with a spatial resolution of 1 km and a time resolution of 8d. The parameter value of the average efficiency of the supply chain network is used to describe the network security status of the food supply chain network when it is destroyed, and the changes in the average efficiency of the food supply chain network under the action of the two types of damage are described. The vegetation index used in the study comes from MODIS and NOAA/AVHRR, so the corresponding pretreatment methods are also different. Pathfinder vegetation index data set the spatial range of this data set as $E70^{\circ}$ – 140° and $N15^{\circ}$ – 55° , including the whole country and parts of Asia. With ten days as the unit, there are 36 scenes a year and a total of 612 scenes from 1984 to 2000.

The specific processing flow of NDVI data is as follows. (1) Use the corresponding software to crop the acquired original images to obtain remote sensing image data of a certain province. (2) According to the official formula, perform band calculation on the image to extract real NDVI data; $NDVI = 0.008 \times (DN - 128)$. (3) The monthly maximum value of the NDVI data obtained in 16 days is synthesized, and finally the monthly vegetation index data are used in the experiment from 1984 to 2000 (the monthly maximum value is from above, and take the maximum value in the middle and late ten days). The historical test is to compare the data obtained by running the model with the known historical data and calculate the error to judge the accuracy of the simulation data. The research area mainly spans three MODIS images, 23 scenes a year, and a total of 1104 scenes of image data from 2001 to 2016. MOD13A2 is a MODIS product data set, including data types such as NDVI, EVI, and reflectance data of each band. The file format is HDF. ENVI software can be used to view the layer contained in the image and the attribute information of the image under the layer and according to the attribute. The calculation formula is $DN \times 0.0001$. (4) Use the maximum synthesis method to eliminate or reduce the influence of factors such as clouds and snow. With the help of the cell statistics tool in ArcGIS for batch processing (Cell Statistics > right click and select batch), the monthly maximum image number is generated, and finally the grain supply sample measurement is obtained. The three-dimensional error surface of the value data is shown in Figure 11.

The crop canopy spectrum at the multispectral crop growth sensor on the node is measured, so the spectrum

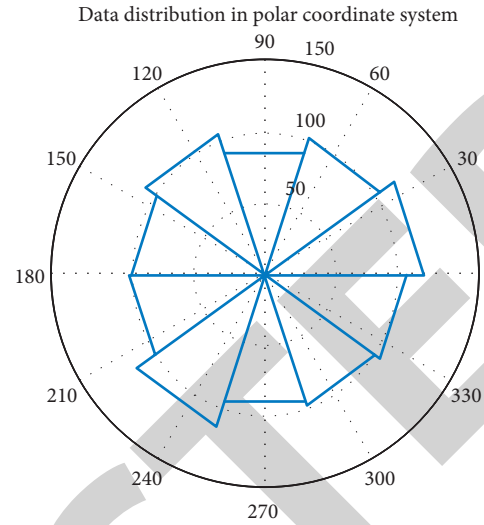


FIGURE 10: Polar coordinate display of grain sample collection data.

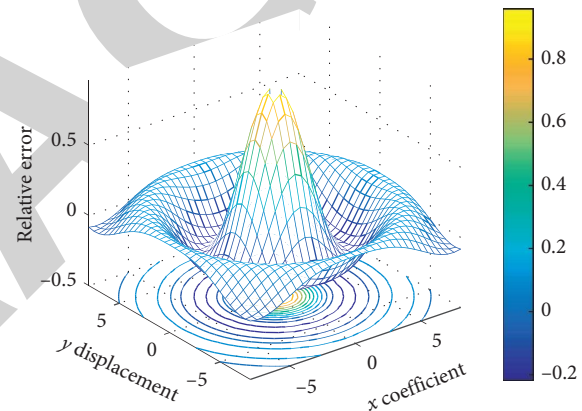


FIGURE 11: The three-dimensional error surface of the measured value data of the grain supply sample.

value measured by the portable crop growth diagnostic instrument is used as the standard value and set to Y815 and Y725, which are the spectral reflectance of the 815 nm band and the 725 nm band, respectively. It realizes man-machine dialogue through a text editor and graphics drawing window and integrates flow chart production, programming, feedback analysis, graphics, and table output. The sum variance SSE is 77.61, and the coefficient of determination R square is 0.98, the mean square error MSE is 2.155, and the root mean square RMSE is 1.468; the cluster analysis of soil moisture sensor BP artificial neural network is shown in Figure 12, and the variance SSE is 69.72, and the coefficient of determination R square is 0.99, the mean square error MSE is 1.74, and the root mean square RMSE is 1.32; from the above, it can be seen that the fitting accuracy of the BP artificial neural network is higher, the error is smaller, and the result of the BP artificial neural network fitting correction is better than the minimum two-fold fitting.

Data fitting is performed on the data set. In the following, we obtain the simulation data of the model by inputting the initial variables of the model and comparing it

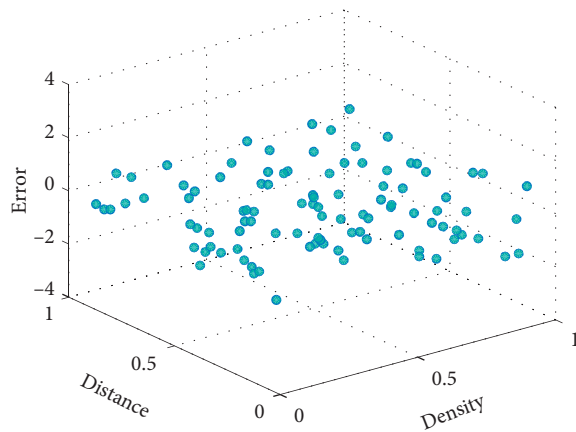


FIGURE 12: Cluster analysis of sample data density.

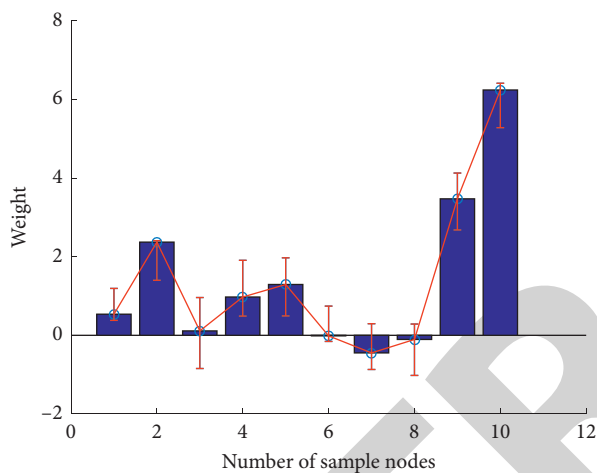


FIGURE 13: The distribution of weights for collecting food supply data.

with the historical data. The number of hidden layer neurons is set to hidden layer size, and the connection weight from the input layer to the hidden layer is $\text{net-w} = [14.5367, -19.3372, 15.3010, -14.3912, 14.9329, 14.0176, 14.0194, 14.4401, 16.2045, 6.1390]$, the threshold from the input layer to the hidden layer is $\text{net-b} = [-12.2353, 17.5935, -4.2518, -0.4229, -1.4041, 0.4284, 4.6125, 10.6248, 8.4058, 21.9747]$, the connection weight of the layer to the output layer is $\text{net-w} = [0.1515, 0.0304, 0.1622, 0.1653, 0.2669, 0.9149, -0.1800, 0.1271, 0.0131, 1.3986]$, the threshold from the hidden layer to the output layer is $\text{net-b} = [1.2808]$; the activation function used in the hidden layer is TANSIG, the output layer function is PURLIN, and the data training function uses the TRAINLM function. After calculating the relative error of the important parameters, as well as the change trend between the two, analyze whether the model has a good simulation effect. Through training, the final number of iterations of the BP artificial neural network is 15 times, and the correlation coefficient between the training data sets is 0.997, the correlation coefficient between the verification data sets is 0.985, the correlation coefficient between the test data sets is 0.946, the overall correlation coefficient is 0.988, and the fitting correlation degree $R^2 = 0.976$, after the BP

artificial neural network. The corrected fitting weight distribution is shown in Figure 13.

4. Conclusion

This paper analyzes the supply relationship of food under digital technology. The farmland Internet of Things has been deployed in the field environment for a long time. The food supply will inevitably be unexpectedly changed by mechanical shocks, external vibrations, electromagnetic interference, and other measurement conditions. The computational complexity of the means clustering analysis algorithm is low, and the effect is obvious when the data are dense and the classification is obvious, while the complexity of the LOF outlier detection algorithm is high, but there is no classification requirement for the perception data when the data classification is not obvious when the LOF outlier detection method is more advantageous. Through the cleaning of the perception data, the noise data and abnormal values in the farmland perception data are removed, and the accuracy of the farmland perception data is improved. According to the characteristics of the food supply chain network, two survivability measures are proposed. The network survivability measure better describes the change characteristics of the network survivability performance. Through the research on digital sensor calibration and perception data cleaning methods, the measurement accuracy of grain digital sensors has been improved, and the accuracy and stability of farmland perception data have been ensured. It is conducive to agricultural production decision-making and managers to better make timely and effective management decisions and response measures based on farmland information perception data. This paper proposes a food supply chain network construction model from the dimensions of the food supply chain network's information flow, logistics, and business flow. At the same time, it analyzed and compared the application of different algorithms in farmland sensor calibration and perception data cleaning and made exploratory research for the further deepening of farmland sensor calibration and perception data cleaning. It is of practical significance to ensure that farmland perception data provide better information support for farmland management and decision-making and to improve the level of informatization, digitization, and refinement of agricultural production.

Data Availability

Data sharing is not applicable to this article as no datasets were generated or analyzed during the current study.

Consent

Informed consent was obtained from all individual participants included in the study references.

Conflicts of Interest

The authors declare that they have no conflicts of interest.

Acknowledgments

This study was funded by the Henan University Philosophy and Social Science Think Tank Research Project (No. 2021-ZKYJ12).

References

- [1] D. Ivanov, A. Dolgui, A. Das et al., “Digital supply chain twins: managing the ripple effect, resilience, and disruption risks by data-driven optimization, simulation, and visibility,” *Journal of Ripple Effects in the Supply Chain*, vol. 22, no. 10, pp. 309–332, 2019.
- [2] B. Y. Ekren, S. K. Mangla, E. E. Turhanlar et al., “Lateral inventory share-based models for IoT-enabled E-commerce sustainable food supply networks,” *Computers & Operations Research*, vol. 130, no. 4, pp. 105–123, 2021.
- [3] M. Lezoche, J. E. Hernandez, M. M. E. A. Díaz et al., “Agri-food 4.0: a survey of the supply chains and technologies for the future agriculture,” *Computers in Industry*, vol. 117, no. 3, pp. 187–192, 2020.
- [4] D. Ivanov, A. Dolgui, and B. Sokolov, “The impact of digital technology and Industry 4.0 on the ripple effect and supply chain risk analytics,” *International Journal of Production Research*, vol. 57, no. 3, pp. 829–846, 2019.
- [5] A. Orozco-Romero, C. Y. Arias-Portela, and J. E. A. Marmolejo-Saucedo, “The use of agent-based models boosted by digital twins in the supply chain: a literature review,” *Journal of Intelligent Computing & Optimization*, vol. 32, no. 23–22, pp. 644–652, 2019.
- [6] S. Singh, R. Kumar, R. Panchal et al., “Impact of COVID-19 on logistics systems and disruptions in food supply chain,” *International Journal of Production Research*, vol. 3, no. 23, pp. 1–13, 2020.
- [7] P. Verboven, T. Defraeye, A. K. Datta, and B. Nicolai, “Digital twins of food process operations: the next step for food process models?” *Current Opinion in Food Science*, vol. 35, no. 3, pp. 79–87, 2020.
- [8] A. Dolgui and D. Ivanov, “Ripple effect and supply chain disruption management: new trends and research directions,” *Journal of Production Research*, vol. 5, no. 31, pp. 29–46, 2021.
- [9] B. Tundys and T. Wiśniewski, “Benefit optimization of short food supply chains for organic products: a simulation-based approach,” *Applied Sciences*, vol. 10, no. 14, pp. 8–12, 2020.
- [10] D. Ivanov and A. Dolgui, “A digital supply chain twin for managing the disruption risks and resilience in the era of Industry 4.0,” *Production Planning & Control*, vol. 8, no. 24, pp. 14–26, 2020.
- [11] D. Balderas, A. Ortiz, E. Méndez et al., “Empowering Digital Twin for Industry 4.0 using metaheuristic optimization algorithms: case study PCB drilling optimization,” *The International Journal of Advanced Manufacturing Technology*, vol. 5, no. 23, 2021.
- [12] Z. Zhu, F. Chu, A. Dolgui et al., “Recent advances and opportunities in sustainable food supply chain: a model-oriented review,” *International Journal of Production Research*, vol. 56, no. 17, pp. 5700–5722, 2018.
- [13] J. Scholz, A. De Meyer, A. S. Marques et al., “Digital technologies for forest supply chain optimization: existing solutions and future trends,” *Environmental Management*, vol. 62, no. 5, pp. 1108–1133, 2018.
- [14] R. Zhong, X. Xu, and L. Wang, “Food supply chain management: systems, implementations, and future research,” *Industrial Management & Data Systems*, vol. 2, no. 15, pp. 8–13, 2017.
- [15] R. D. Tordecilla, A. A. Juan, J. R. Montoya-Torres et al., “Simulation-optimization methods for designing and assessing resilient supply chain networks under uncertainty scenarios: a review,” *Simulation Modelling Practice and Theory*, vol. 106, no. 14, pp. 102–166, 2021.
- [16] J. Lohmer, N. Bugert, and R. Lasch, “Analysis of resilience strategies and ripple effect in blockchain-coordinated supply chains: an agent-based simulation study,” *International Journal of Production Economics*, vol. 228, no. 34, pp. 107–182, 2020.
- [17] C. N. Verdouw and J. W. Kruize, “Digital twins in farm management: illustrations from the FIWARE accelerators SmartAgriFood and Fractals,” *Journal of Precision Agriculture Digital*, vol. 32, no. 7, pp. 1–5, 2017.
- [18] T. Defraeye, C. Shrivastava, T. Berry et al., “Digital twins are coming: will we need them in supply chains of fresh horticultural produce,” *Trends in Food Science & Technology*, vol. 42, no. 17, pp. 11–15, 2021.
- [19] D. Ivanov, “Lean resilience: AURA (Active Usage of Resilience Assets) framework for post-COVID-19 supply chain management,” *The International Journal of Logistics Management*, vol. 132, no. 71, pp. 21–35, 2021.
- [20] P. W. Khan, Y. C. Byun, and N. Park, “IoT-Blockchain enabled optimized provenance system for food industry 4.0 using advanced deep learning,” *Sensors*, vol. 20, no. 10, pp. 29–34, 2020.
- [21] M. M. Queiroz, D. Ivanov, A. Dolgui et al., “Impacts of epidemic outbreaks on supply chains: mapping a research agenda amid the COVID-19 pandemic through a structured literature review,” *Annals of Operations Research*, vol. 52, no. 37, pp. 1–45, 2020.
- [22] V. Todorovic, M. Maslaric, S. Bojic et al., “Solutions for more sustainable distribution in the short food supply chains,” *Sustainability*, vol. 10, no. 17, pp. 31–55, 2018.
- [23] Y. Liu, Q. Zhu, and S. Seuring, “New technologies in operations and supply chains: implications for sustainability,” *International Journal of Production Economics*, vol. 22, no. 9, pp. 81–95, 2020.
- [24] M. Ben-Daya, E. Hassini, Z. Bahroun et al., “The role of internet of things in food supply chain quality management: a review,” *Quality Management Journal*, vol. 2, no. 31, pp. 11–25, 2020.
- [25] J. Sharma, M. Tyagi, and A. Bhardwaj, “Parametric review of food supply chain performance implications under different aspects,” *Journal of Advances in Management Research*, vol. 32, no. 9, pp. 6–15, 2020.
- [26] W. Liu, W. Zhang, B. Dutta et al., “Digital twinning for productivity improvement opportunities with robotic process automation: case of greenfield hospital,” *International Journal of Mechanical Engineering and Robotics Research*, vol. 9, no. 2, pp. 258–263, 2020.
- [27] M. Jayakrishnan, A. K. Mohamad, and A. Abdullah, “Enterprise architecture embrace digital technology in Malaysian transportation industry,” *International Journal of Engineering and Advanced Technology*, vol. 8, no. 4, pp. 852–859, 2019.
- [28] B. Zhang, D. Xu, Y. Liu et al., “Multi-scale evapotranspiration of summer maize and the controlling meteorological factors in north China,” *Agricultural and Forest Meteorology*, vol. 216, pp. 1–12, 2016.
- [29] M. Liu, C. Li, C. Cao et al., “Walnut fruit processing equipment: academic insights and perspectives,” *Food Engineering Reviews*, vol. 215, pp. 1–36, 2021.

- [30] J. Yang, M. Xi, B. Jiang et al., “robust six degrees of freedom estimation for IIoT based on multibranch network,” *IEEE Transactions on Industrial Informatics*, vol. 17, no. 4, pp. 2767–2775, 2021.
- [31] F. Orujov, R. Maskeliūnas, R. Damaševičius et al., “Smartphone based intelligent indoor positioning using fuzzy logic,” *Future Generation Computer Systems*, vol. 89, pp. 335–348, 2018.
- [32] J. H. Wu, W. Wei, L. Zhang et al., “Risk assessment of hypertension in steel workers based on LVQ and Fisher-SVM deep excavation,” *IEEE Access*, vol. 7, pp. 23109–23119, 2019.
- [33] J. Guo, Y. Zhao, Y. Jiang et al., “Coverage guided differential adversarial testing of deep learning systems,” *IEEE Transactions on Network Science and Engineering*, vol. 1, 2020.
- [34] J. Wen, J. Yang, B. Jiang et al., “Big data driven marine environment information forecasting: a time series prediction network,” *IEEE Transactions on Fuzzy Systems*, vol. 2, pp. 21–28, 2020.
- [35] J. Yang, J. Zhang, and H. Wang, “Urban traffic control in software defined internet of things via a multi-agent deep reinforcement learning approach,” *IEEE Transactions on Intelligent Transportation Systems*, vol. 3, pp. 18–26, 2020.